Talanta 182 (2018) 125–130

Contents lists available at ScienceDirect

Talanta

journal homepage: www.elsevier.com/locate/talanta

Highly sensitive and selective detection of Pb^{2+} using a turn-on fluorescent aptamer DNA silver nanoclusters sensor

Baozhu Zhang[a,b], Chunying Wei[a,*]

[a] Key Laboratory of Chemical Biology and Molecular Engineering of Ministry of Education, Institute of Molecular Science, Shanxi University, Taiyuan 030006, PR China
[b] College of Chemistry and Chemical Engineering, Jinzhong University, Yuci 030619, PR China

ARTICLE INFO

Keywords:
DNA-Ag NCs
Aptamer
G-quadruplex
Pb^{2+}

ABSTRACT

A novel turn-on fluorescent biosensor has been constructed using C-PS2.M-DNA-templated silver nanoclusters (Ag NCs) with an average diameter of about 1 nm. The proposed approach presents a low-toxic, simple, sensitive, and selective detection for Pb^{2+}. The fluorescence intensity of C-PS2.M-DNA-Ag NCs enhances significantly in the presence of Pb^{2+}, which is attributed to the special interaction between Pb^{2+} and its aptamer DNA PS2.M. Pb^{2+} induces the aptamer to form G-quadruplex and makes two darkish DNA/Ag NCs located at the 3′ and 5′ terminus close, resulting in the fluorescence light-up. Moreover, Pb^{2+} can be detected as low as 3.0 nM within a good linear range from 5 to 50 nM (R = 0.9862). Furthermore, the application for detection of Pb^{2+} in real water samples further demonstrates the reliability of the sensor. Thus, this sensor system shows a potential application for monitoring Pb^{2+} in environmental samples.

1. Introduction

Pb^{2+}, as a highly toxic heavy metal ion, causes adverse health effects to humans, including kidney, liver, and nervous system diseases, high blood pressure in adults, and delayed physical and mental development in infants and children [1,2]. Thus, it is increasingly important and necessary for the health of human beings to develop a highly sensitive and selective method for the detection of Pb^{2+} in drinking water and biosystem. Although instrumental techniques for Pb^{2+} detection are widely used, such as atomic absorption spectrometry (AAS) [3,4], inductively coupled plasma atomic emission spectroscopy (ICP-AES) [5,6], and inductively coupled plasma mass spectrometry (ICP-MS) [7], they suffer from expensive and sophisticated instruments and/or complicated sample preparation processes. Therefore, to overcome these limitations and drawbacks, a variety of sensors such as colorimetry [8,9], fluorescence [10,11], and electrochemistry [12,13] have been developed to rapidly detect Pb^{2+} by utilizing organic fluorescent dyes, oligonucleotides, or Pb^{2+}-dependent RNA cleaving DNAzymes. Especially, conjugated nanomaterials are growing attention for detection of diverse metal ions based on their specific functionality by colorimetric method. For example, Awual's group has performed a lot of excellent researches in the detection and removal of diverse heavy metal ions [14–18] including Pb^{2+} [1,2,19–22] using ligands doped conjugate adsorbents. In addition, Pb^{2+} is able to induce the structural transition of a guanine (G)-rich single-stranded oligonucleotide into a G-quadruplex [23] that consists of planar stacks of four guanines stabilized by Hoogsteen hydrogen bonding [24], and some of biosensors of Pb^{2+} ions have been designed by exploiting this feature [25,26]. However, some disadvantages still existed, such as high toxicity, poor aqueous solubility, and complicated synthesis procedures [27]. Recently, fluorescent metal nanocluster (NCs) for Pb^{2+} sensing have drawn increasing attention because of their good biocompatibility, low cost, simple operation, and high sensitivity and selectivity [28–30]. Nevertheless, most of nanocluster sensors belong to “on-off’ and are not ideal sensors for being possibly interfered by various factors. Thus, the development of a turn-on fluorescent metal nanocluster probe for detecting Pb^{2+} is necessary.

Fluorescent noble metal nanoclusters, consisting of a few to roughly a hundred atoms, have attracted a great deal of interest for their unique chemical and physical features, such as owning sizes comparable to the Fermi wavelength of electrons and showing molecule-like properties, including discrete electronic transitions and strong fluorescence [31]. However, without stabilizer noble metal nanoclusters would strongly interact with each other and aggregate irreversibly to reduce their surface energy [32]. A number of methods have been developed to generate noble metal nanoclusters in the past decade [33,34], and DNA oligonucleotides, polymers, dendrimers and thiols can be exploited for stabilizing fluorescent metal nanoclusters [35]. Among these small molecules, DNA oligonucleotides provide a versatile scaffold for preparing fluorescent nanoclusters due to possessing optimizable strand

* Corresponding author.
E-mail address: weichuny@sxu.edu.cn (C. Wei).

https://doi.org/10.1016/j.talanta.2018.01.061
Received 7 September 2017; Received in revised form 21 December 2017; Accepted 27 January 2018
Available online 31 January 2018
0039-9140/

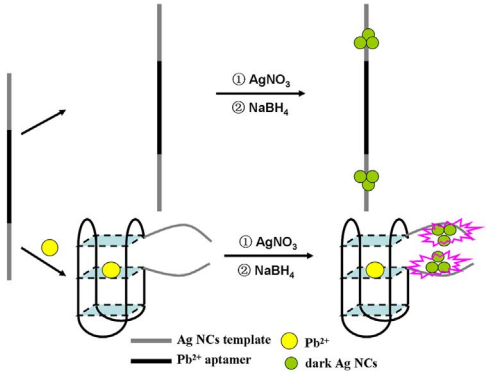

Scheme 1. Schematic illustration of the sensing method for the detection of Pb^{2+} by using ssDNA-scaffolded silver nanoclusters combined with PS2.M aptamer.

length and base sequence [36,37]. Particularly, DNA-scaffolded silver nanoclusters (DNA-Ag NCs) [38], as a new class of promising fluorescent nanomaterials and an ideal alternative to organic dyes and quantum dots, have been successfully applied in biosensing [39,40] and bioimaging [41,42] owing to their strong fluorescence emission, lower toxicity, excellent photophysical properties, and good biocompatibility.

It is found that the fluorescence intensity can enhance largely when two darkish DNA–Ag NCs are closed each other by their complementary linkers [43], herein, we construct a Pb^{2+} biosensor by a similar mode, and the working principle of the sensor is depicted as Scheme 1. DNA template consists of two segments: one is the Ag NCs-nucleation segment at the two termini, and the other is the aptamer segment of Pb^{2+} in the middle of DNA template. Upon addition of Pb^{2+}, the high specificity and affinity of the Pb^{2+} aptamer to Pb^{2+} results in the conformational change of the aptamer and makes the two darkish DNA–Ag NCs close, which enhances largely the fluorescence of Ag NCs and enables the sensitive, specific and turn-on detection of Pb^{2+}.

2. Experimental

2.1. Reagents and apparatus

The oligonucleotides employed in this work are provided by Sangon Biotechnology Inc. (Shanghai, China). The sequences and names of DNA are listed in Table S1. Sodium borohydride ($NaBH_4$, 98%), silver nitrate ($AgNO_3$, 99.8%), acetic acid, $CaCl_2$, $Cd(NO_3)_2$, $Co(NO_3)_2$, $Cr(NO_3)_3$, $Cu(NO_3)_2$, $Fe(NO_3)_3$, $Hg(NO_3)_2$, KNO_3, $Mg(NO_3)_2$, $Mn(NO_3)_2$, $NaNO_3$, $Pb(NO_3)_2$, $TbCl_3$, and $Zn(NO_3)_2$, are purchased from Aladdin Bio-chem technology Co. Ltd. (Shanghai, China). Tris (Tris-(hydroxymethyl) aminomethane) is obtained from Sigma-Aldrich (Shanghai, China). The standard reference materials for river sediment (GBW07310) and soil (GBW07403) are obtained from the National Institute of Metrology (Beijing, China). All chemical reagents are the analytical grade and used as received without further purification. All solutions are prepared using Milli-Q water.

Fluorescence measurements are performed using Fluoromax-4 Spectrofluorometer (Horiba Jobin Yvon Inc., France) or a Cary Eclipse Fluorescence spectrophotometer (Varian Inc. CA) at room temperature, and the slit widths are 5.0 nm and 10 nm for excitation and emission, respectively. UV–vis absorption spectra are recorded at room temperature with a Cary 50 Bio spectrophotometer (Varian Inc., CA). CD spectra are performed at room temperature on a Chirascan Circular Dichroism Spectrometer (Applied Photophysics Ltd., Surrey, UK), and the spectrum is obtained within the range of 220–320 nm at 1 nm intervals employing 1 mm optical path-length quartz cell and an instrument scanning speed of 120 nm/min. Time-resolved fluorescence measurements were performed using FL920 fluorescence lifetime spectrometer (Edinburgh Instruments, Livingston, UK) operating in the time-correlated single photon counting (TCSPC) mode using a semiconductor laser (405 nm) as the excitation source. Commercial software by Edinburgh Instruments is used for data analyses. When $\sum_{i=1}^{n} A_i = 1$, the average excited state lifetime is expressed by the equation $\tau_{avg} = \sum_{i=1}^{n} A_i \tau_i$. The reported spectrum of each sample represents the average of three scans. The morphologies and average size of the DNA–Ag NCs are recorded by using a JEOL JEM-2100 transmission electron microscope with an acceleration voltage of 200 kV. The real samples are analyzed by the classic inductively coupled plasma-mass spectrometry (ICP-MS) on a NexION350X instrument (PerkinElmer Inc. USA).

2.2. Sample preparation

The certified reference material (GBW07310 and GBW07403) is digested according to the previous literature [44]. 0.05 g of sample powder is accurately weighed into a 50 mL container and 4.0 mL of concentrated nitric acid and 12 mL of concentrated hydrochloric acid (aqua regia) is added. A watch glass is put on the container and the mixture is evaporated on a hot plate at 95 °C almost to dryness. Then 8.0 mL of aqua regia is added to the residue and the mixture is again evaporated to dryness (but not baked). After cooling, the resulting mixture is filtered through a 0.45 μm polytetrafluo-roethylene (PTFE) millipore filter. The sample is diluted to 50 mL with double distilled water and analyzed by the proposed procedure.

2.3. Preparation of DNA-Ag NCs and fluorescence assay of Pb^{2+}

DNA-Ag NCs are synthesized according to our previous reported method [38]. Briefly, The DNA oligonucleotides (0.3 μM) with various concentrations (0–500 nM) of Pb^{2+} ions in tris-acetate buffer (5 mM, pH 7.0) were first heated at 85 °C for 15 min and then gradually cooled to 4 °C. Then $AgNO_3$ was added to the DNA solution, and the mixture was kept away from light at 4 °C for 20 min, followed by reduction with the freshly prepared $NaBH_4$ and by the vigorous shaking of the solution for 1 min. The final concentrations of DNA, $AgNO_3$, and $NaBH_4$ were 0.3, 1.8, and 1.8 μM, respectively. The final mixture was kept in the dark at 4 °C for 1 h. The incubation time was calculated from after the addition of $NaBH_4$. The fluorescent spectrum of each sample was recorded at room temperature.

2.4. Selective detection of Pb^{2+}

To investigate whether the other metal ions could interfere with the detection of Pb^{2+}, the selectivity of the fluorescence assay was measured. The metal ions such as Na^+, K^+, Ca^{2+}, Cr^{3+}, Co^{2+}, Cu^{2+}, Pb^{2+}, Mn^{2+}, Mg^{2+}, Cd^{2+}, Hg^{2+}, Zn^{2+}, Tb^{3+} and Fe^{3+} were used, and the concentrations of Pb^{2+} and the other metal ions were 0.1 and 1 μM, respectively. The assay method was same as that of Pb^{2+}.

2.5. Circular dichroism measurements

C-PS2.M (5.0 μM) with 20 nM Pb^{2+} in tris-acetate buffer (5 mM, pH 7.0) were first heated at 85 °C for 15 min and gradually cooled to 4 °C. Then C-PS2.M-DNA-Ag NCs were prepared according to the method described above (see Section 2.3), subsequently, CD spectra were measured.

2.6. Analytical applications

To demonstrate the practical application of the C-PS2.M-DNA-Ag NCs detection system, metal ions in tap water and lake water (from Shanxi University) were detected by using this sensing system. The samples were spiked with standard Pb^{2+} solution at different concentration levels, and the actual samples were measured using the same approach as described above.

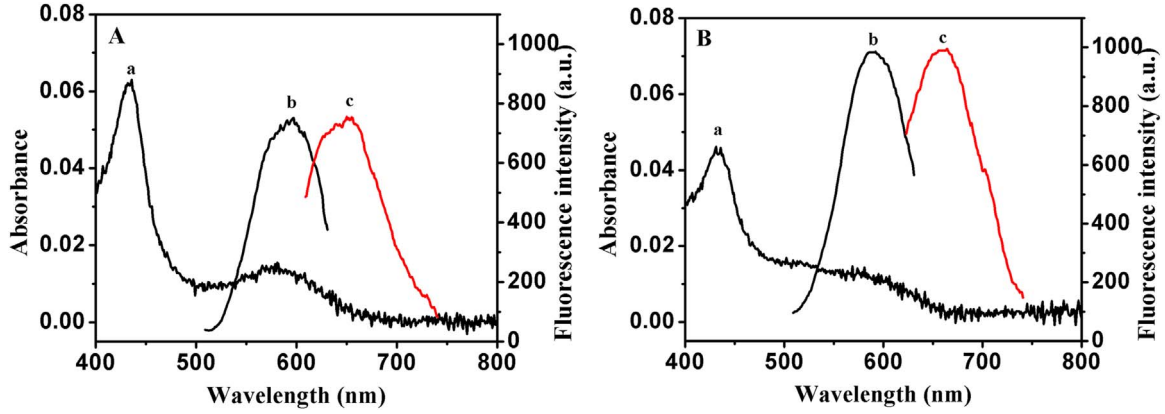

Fig. 1. Optical characterization of C-PS2.M-DNA-Ag NCs without (A) and with 10 nM Pb^{2+} (B). Absorption (curve a), excitation (curve b), and emission (curve c) spectra of the as-prepared C-PS2.M-DNA-Ag NCs.

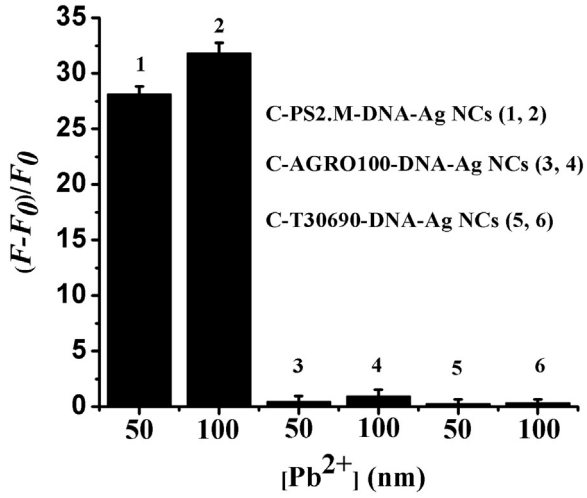

Fig. 2. Selectivity of Pb^{2+} aptamers. Relative fluorescence intensity $[(F-F_0)/F_0]$ of different ssDNA-Ag NCs in the presence of 50 and 100 nM Pb^{2+}. F_0 and F are the maximum emission intensity of the ssDNA-Ag NCs before and after the addition of Pb^{2+}, respectively.

3. Results and discussion

3.1. Optical characterization of ssDNA-Ag NCs

The creation of ssDNA-Ag NCs without formation of large nanoparticles is due to the high affinity of Ag^+ for cytosine, and the as-prepared Ag NCs based on the template of C-rich ssDNA exhibit the hopeful photophysical parameters [45,46]. Herein, the C-rich ssDNA-Ag NCs were synthesized based on the three different DNA templates, namely C-PS2.M-DNA, C-T30695-DNA, and C-ARGO100-DNA (Table S1). Among them the aptamers of Pb^{2+} (the middle segment of the template, italic) are G-rich sequences PS2.M [47–49], T30695 [47,50,51], and ARGO100 [47,50], respectively, while the C-rich segments at the 5′ and 3′ ends (bold) are same. In the case of C-PS2.M and C-T30695 DNAs, the TTT and AAA linkers (underline) are inserted between the C-rich and the aptamer. The optical characterizations of C-PS2.M-DNA-Ag NCs in the absence and presence of 10 nM Pb^{2+} are shown in Fig. 1. Both UV–vis absorption spectra of C-PS2.M-DNA-Ag NCs alone (Fig. 1A, curve a) and with 10 nM Pb^{2+} (Fig. 1B, curve a) show the two peaks at 432 and 585 nm. The peak at 432 nm is characteristic plasmon absorption band of Ag nanoparticles [52,53], and the peak at 585 nm should be attributed to the absorption band of Ag NCs [38]. Upon excitation at 585 nm (Fig. 1A and B, curve b), both C-PS2.M-DNA-Ag NCs alone and with 10 nM Pb^{2+} present the same maximum emission peak at 650 nm (Fig. 1A and B, curve c), but the fluorescence intensity of the latter is stronger than that of the former, which is attributed to the reason that PS2.M DNA folds into G-quadruplex structure in the presence of Pb^{2+} to make two darkish DNA–Ag NCs close and result in the fluorescence lighting up (Scheme 1). It is reported that the Pb^{2+}-stabilized PS2.M G-quadruplex is a monomolecular antiparallel conformation, and a strong positive band at 312 nm and a weak negative band at 265 nm are observed in the CD spectrum [47,49]. To confirm the conformation of C-PS2.M-DNA-Ag NCs in the presence of 20 nM Pb^{2+}, CD spectra were measured. As shown in Fig. S1, the CD spectrum presents a broad positive band centered at 270 nm, together with a shoulder peak at about 290 nm and a negative band at 240 nm. The positions of both peaks obviously deviated from those in PS2.M G-quadruplex, which might be attributed to the ssDNA-Ag NCs containing 15 bases located at 3′- and 5′-terminus that shift the peak position of G-quadruplex.

In addition, the UV–vis absorption spectra and the excitation and emission spectra of C-ARGO100-DNA-Ag NCs and C-T30695-DNA-Ag NCs are also shown in Figs. S2 and S3, respectively. Upon excitation at 570 nm, C-ARGO100-DNA-Ag NCs in the absence and presence of 10 nM Pb^{2+} show a maximum emission at 625 nm (curves b and c, Figs. S2A and S2B). The fluorescence intensity of the latter is slightly stronger than that of the former. C-T30695-DNA-Ag NCs alone and with 10 nM Pb^{2+} show a maximum emission at 620 nm upon excitation at 560 nm (curves b and c, Figs. S3A and S3B), similarly, the fluorescence intensity of the latter is a little stronger than that of the former.

As illustrated in Figs. 2 and S4A, the fluorescence intensity of C-PS2.M-DNA-Ag NCs enhances more than 30 times in the presence of 100 nM Pb^{2+} compared to that without Pb^{2+}, while the fluorescence intensities of C-ARGO100- and C-T30695-DNA Ag NCs only increase about 2.2 and 1.5 times at the same condition, respectively (Figs. 2, S4B and S4C). The aptamers of Pb^{2+} PS2.M, ARGO100, and T30695 (Table S1) would fold into a G-quadruplex structure in the presence of Pb^{2+}. However, it is reported that their G-quadruplex conformations are different in the presence of Pb^{2+}. PS2.M forms an intramolecular antiparallel structure, while both T30695 and ARGO100 mainly adopt a monomeric parallel structure [47,50]. Thus, the 5′-termini and 3′-termini of C-T30695-DNA and C-ARGO100-DNA locate at the opposite site and the fluorescence intensity of the DNA-Ag NCs is weak. On the contrary, the distance between 5′-terminus and 3′-terminus in the C-PS2.M-DNA is close in the presence of Pb^{2+}, expectedly, the fluorescence intensity of the DNA-Ag NCs enhances. Thus, C-PS2.M-DNA-Ag NCs are used for the following experiments.

3.2. Detection of Pb^{2+}

Firstly, the change of fluorescence intensity of C-PS2.M-DNA-Ag

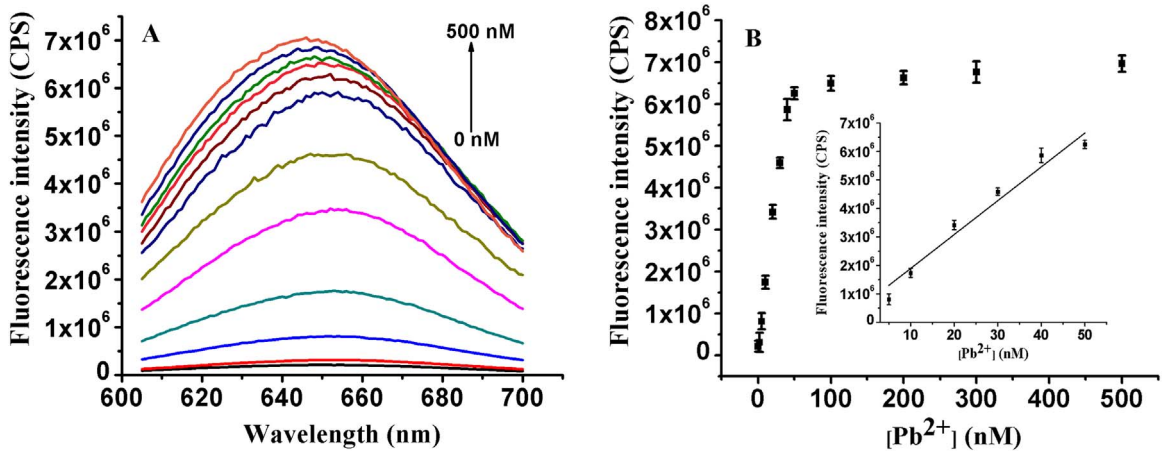

Fig. 3. Detection of Pb^{2+}. (A) Changes of fluorescence emission spectra (λ_{ex} = 585 nm) of C-PS2.M-DNA-Ag NCs upon the addition of Pb^{2+} in different concentrations. (B) Changes of maximum fluorescence emission intensity at a wavelength of 650 nm as a function of Pb^{2+} concentration. The insert shows the linear range of 5–50 nM (R = 0.9862). The error bars represent the standard deviation of three independent measurements.

Table 1
Comparison of optical sensors for the detection of Pb^{2+}.

Detection methods	Strategy	LOD	Linear range	Refs.
Colorimetry	The mesoporous silica doped by ammonium(4-chloro-2-mercaptophenyl)carbamodithioate (ACMPC)	1.2 μg/L	0.002–0.10 mg/L	[20]
Colorimetry	A test strip based on multifunctionalized AuNPs by DNAzyme and barcode DNA	20 nM	Not reported	[55]
Fluorescence	Fluorescent DNA molecular device based on a DNA duplex-quadruplex exchange	20 nM	20 nM to 1 μM	[56]
Fluorescence	Fluorescent detection with an RNA aptamer folds into G4 conformation	6 nM	5–500 nM	[57]
Fluorescence	NSET between FAM and AuNPs by the formation of G-quadruplex	10 nM	12.5–100 nM	[58]
Fluorescence	Label-free fluorescent sensor based on G-quadruplex formation	18 nM	0–480 nM	[59]
Fluorescence	DNA-Ag NCs	3 nM	5–50 nM	This work

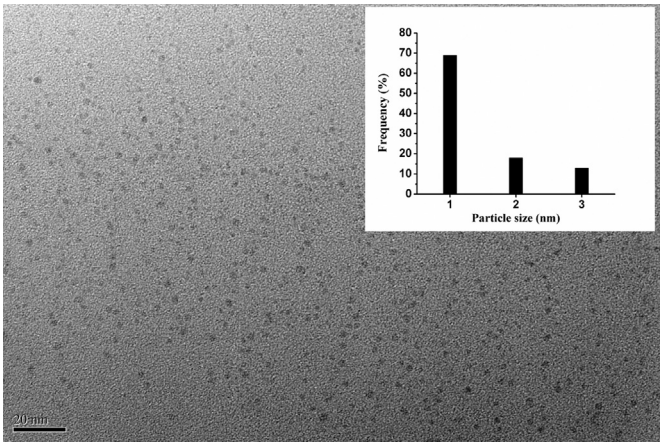

Fig. 4. TEM images of C-PS2.M-DNA-Ag NCs in the presence of 10 nM Pb^{2+}. The inset shows the size distribution histogram.

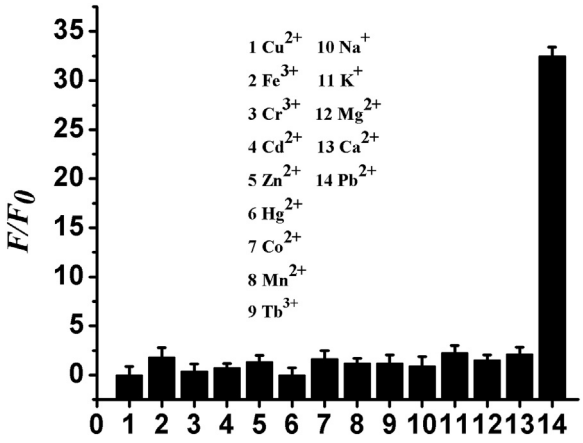

Fig. 5. Selectivity of C-PS2.M-DNA-Ag NCs for the detection of Pb^{2+}. Relative fluorescence emission intensity (F/F_0) of PS2.M-DNA-Ag NCs upon the addition of 0.1 μM Pb^{2+} and 1 μM other different metal ions. F_0 and F are the maximum emission intensity of the DNA-Ag NCs before and after addition of metal ions.

NCs after addition of 10 nM Pb^{2+} with the increasing incubating time was studied. As shown in Fig. S5, after addition of 10 nM Pb^{2+} the fluorescence intensity of C-PS2.M-DNA-Ag NCs gradually increases and gets to the maximum value at 1.5 h, then decreases with the increasing incubation time. So the optimal detection time for Pb^{2+} is 1.5 h.

To evaluate the interactions of C-PS2.M-DNA-Ag NCs with Pb^{2+}, different concentrations of Pb^{2+} were added into the solution of C-PS2.M-DNA (see Section 2.3), and the fluorescence emission of the as-prepared C-PS2.M-DNA-Ag NCs was determined. As shown in Fig. 3, the fluorescence intensity of C-PS2.M-DNA-Ag NCs increases gradually with the increasing concentration of Pb^{2+}, a good linear relationship is observed in the range of 5–50 nM (R = 0.9862, the regression equation is $F = 402481.7 + 127312.0C_{Pb^{2+}}$) with a detection limit (LOD) of 3.0 nM based on $3\sigma_0/\sigma$, where σ_0 is the standard deviation of background and σ is the sensitivity that is 127312.0. This LOD meets the Pb^{2+} detection requirement for drinking water of the U.S. Environmental Protection Agency (EPA, 70 nM) and the International Agency for Research on Cancer (IARC, 48.26 nM) in food and water [54]. For comparison, the linear ranges and detection limits for Pb^{2+} detection by different sensors are listed in Table 1. The LOD of our proposed method is comparable to those of previously reported sensors for Pb^{2+} based on the methods of colorimetry and fluorescence [20,55–59].

Furthermore, the TEM image of C-PS2.M-DNA-Ag NCs in the presence of Pb^{2+} was measured. As indicated in the Fig. 4, C-PS2.M-DNA-Ag NCs uniformly distributed with the average size of about 1 nm (the

Table 2
The concentration of Pb^{2+} in real water samples detected using the proposed Pb^{2+} sensor system and ICP-MS (N = 3).

Samples	Spiked (nM)	C-PS2.M-DNA-AgNCs measured (nM) mean[a] ± *SD*[b]	C-PS2.M-DNA-AgCs recovery (%)	ICP-MS measured (nM) mean[a] ± SD[b]	Recovery (%)
Lake water 1	10	10.55 ± 0.14	105.5	9.867 ± 0.12	98.67
Lake water 2	30	29.06 ± 0.07	96.90	30.09 ± 0.09	100.3
Tap water 1	10	9.745 ± 0.06	97.45	10.06 ± 0.15	100.6
Tap water 2	30	29.06 ± 0.12	96.90	29.85 ± 0.07	99.50

[a] The mean of three determinations.
[b] *SD* = standard deviation.

inset of Fig. 4), which is according with the core size below 2.0 nm for metal nanoclusters [60]. In addition, the fluorescence lifetimes at 650 nm of C-PS2.M-DNA-Ag NCs before and after interaction with the target Pb^{2+} are also measured (Fig. S6). The fluorescence transients of C-PS2.M-DNA-Ag NCs present tri-exponential time constants (Table S2) with an about 3 ns of average lifetime. The average lifetime of C-PS2.M-DNA-Ag NCs is similar to the reported results based on DNA-templated fluorescence Ag NCs [38,61,62], while it is longer than that of Ag NCs capped by GSH with average lifetime of 1.026 ns [63] and much shorter than those of AgNCs prepared by dihydrolipoic acid with a very high lifetime of 39.96 μs [64], which should be attributed to the Ag NCs protected by the different protective layers. The results demonstrate that there are no obvious changes in the average fluorescence lifetimes of C-PS2.M-DNA-Ag NCs in the absence and presence of different concentrations of Pb^{2+}, indicating a static quenching mechanism.

3.3. Selectivity of C-PS2.M-DNA-Ag NCs for detecting Pb^{2+} and pH dependence

To investigate the specificity of C-PS2.M-DNA-Ag NCs sensing platform, the sensing system was challenged by monitoring other metal ions, e.g., Cu^{2+}, Fe^{3+}, Cr^{3+}, Cd^{2+}, Zn^{2+}, Hg^{2+}, Mn^{2+}, Co^{2+}, Tb^{3+}, Na^{+}, K^{+}, Mg^{2+}, and Ca^{2+} with the same assay format as that in the case of Pb^{2+}. As indicated in Fig. 5, only the target Pb^{2+} (0.1 μM) causes a significant increase of the fluorescent intensity (F/F_0) even if the high-concentrations of other metal ions (1 μM) are added. The results clearly demonstrate that this sensing platform is highly selective for target Pb^{2+}, and the proposed approach can be used to detect Pb^{2+} specifically.

The influence of pH value on the sensitivity of the C-PS2.M-DNA-Ag NCs for detection of Pb^{2+} was further investigated. As shown in Fig. S7, the relative fluorescence intensity of C-PS2.M-DNA-Ag NCs with 10 nM Pb^{2+} increases with the increasing pH values from 5 to 7 and then decreases from 7 to 9. When the pH value is 7, the relative fluorescence intensity gets to a maximum value, indicating that the performance of this sensor is the best under the neutral pH condition.

3.4. Analytical applications

To further demonstrate the application potential of our strategy for analysis of tap water and lake water (from Shanxi University). The water samples were filtered three times through qualitative filter paper and centrifuged, and the supernatants were used for the quantitative analysis. Pb^{2+} is not detected in these real samples because the concentration of Pb^{2+} is much lower than the detection limit of C-PS2.M-DNA-Ag NCs sensing system. Therefore, the samples are spiked with standard Pb^{2+} solution at different concentration levels. The average values of three replicate determination results were listed in Table 2. For comparison, the amount of Pb^{2+} was also measured by the classic ICP-MS method (Table 2). It is found that the average recoveries of Pb^{2+} in the actual samples for the proposed method and the ICP-MS method are in the range of 96.9–105.5% and 98.67–100.6%, respectively. Obviously, there was no significant difference between the results obtained from the two methods, indicating that C-PS2.M-DNA-Ag NCs sensing platform could be applied for the quantitative determination of Pb^{2+} in actual water samples.

3.5. Evaluation of the proposed sensor

Accuracy, repeatability and reproducibility are important factors to evaluate the good performance of a sensor. The accuracy and reliability of the proposed probe was evaluated by the quantification of Pb^{2+} in a series of certified reference materials, including GBW07310 and GBW07403. The obtained results (Table S3) are in good agreement with the certified values, which confirms that the proposed method is suitable for the determination of environmental samples. The repeatability of the sensor was also tested with tap water spiked 15 nM Pb^{2+}. As shown in Table S4, the average relative standard deviation (*RSD*) in tap water for the proposed sensor is in the range of 0.47–0.92%. Similarly, the reproducibility of the method was further measured. Milli-Q water, tap water, or lake water spiked 20 nM Pb^{2+} was performed by two persons in two different laboratories, and the results are listed in Table S5. The *RSD* values in three kinds of solution are from 0.40% to 0.75%. As illustrated above, the *RSD* values of both results are less than 5%, demonstrating that the repeatability and reproducibility of the as-presented analytical method are acceptable.

4. Conclusions

In summary, a novel strategy for the detection of Pb^{2+} has been developed using C-PS2.M-DNA-stabilized Ag NCs as a turn-on fluorescent probe based on Pb^{2+} induced conformation transition of PS2.M DNA. This sensing system presents high selectivity and sensitivity, with a LOD of 3.0 nM. Meanwhile, the sensor also gives good accuracy, repeatability and reproducibility. Importantly, this novel sensing method is low-cost and environmentally friendly due to the good biocompatibility of DNA-Ag NCs. In addition, it has also been successfully applied in the detection of Pb^{2+} in actual water samples, thus the C-PS2.M-DNA-Ag NCs sensing system is a potential approach for Pb^{2+} sensing in environmental samples.

Appendix A. Supplementary material

Supplementary data associated with this article can be found in the online version at.

Acknowledgments

This work was supported by the National Natural Science Foundation of China (21171108); and Shanxi Provincial Fund for Natural Sciences (201601D011026).

Appendix A. Supplementary material

Supplementary data associated with this article can be found in the online version at http://dx.doi.org/10.1016/j.talanta.2018.01.061.

References

[1] M.R. Awual, M.M. Hasan, A novel fine-tuning mesoporous adsorbent for simultaneous lead(II) detection and removal from wastewater, Sens. Actuators B: Chem. 202 (2014) 395–403.
[2] M.R. Awual, M.M. Hasan, A. Shahat, Functionalized novel mesoporous adsorbent for selective lead(II) ions monitoring and removal from wastewater, Sens. Actuators B: Chem. 203 (2014) 854–863.
[3] Y.Y. Zhou, L. Tang, G.G. Zeng, C. Zhang, Y. Zhang, X. Xie, Current progress in biosensors for heavy metal ions based on DNAzymes/DNA molecules functionalized nanostructures: a review, Sens. Actuators B: Chem. 223 (2016) 280–294.
[4] S. Dolati, M. Ramezani, K. Abnous, S.M. Taghdisi, Recent nucleic acid based biosensors for Pb^{2+} detection, Sens. Actuators B: Chem. 246 (2017) 864–878.
[5] J.S.F. Pereira, C.L. Knorr, L.S.F. Pereira, D.P. Moraes, J.N.G. Paniz, E.M.M. Flores, G. Knapp, Evaluation of sample preparation methods for polymer digestion and trace elements determination by ICPMS and ICPOES, J. Anal. At. Spectrom. 26 (2011) 1849–1857.
[6] A. Sixto, M. Fiedoruk-Pogrebniak, M. Rosende, D. Cocovi-Solberg, M. Knochen, M. Miró, A mesofluidic platform integrating restricted access-like sorptive microextraction as a front end to ICP-AES for the determination of trace level concentrations of lead and cadmium as contaminants in honey, J. Anal. At. Spectrom. 31 (2016) 473–481.
[7] S. Su, B. Chen, M. He, B. Hu, Graphene oxide-silica composite coating hollow fiber solid phase microextraction online coupled with inductively coupled plasma mass spectrometry for the determination of trace heavy metals in environmental water samples, Talanta 123 (2014) 1–9.
[8] A. Malek, T. Thomas, E. Prasad, Visual and optical sensing of Hg^{2+}, Cd^{2+}, Cu^{2+} and Pb^{2+} in water and its beneficiation via gettering in nanoamalgam form, ACS Sustain. Chem. Eng. 4 (2016) 3497–3503.
[9] W. Chu, Y. Zhang, D. Li, C.J. Barrow, H. Wang, W. Yang, A biomimetic sensor for the detection of lead in water, Biosens. Bioelectron. 67 (2015) 621–624.
[10] X. Zhao, R. Kong, X. Zhang, H. Meng, W. Liu, W. Tan, G. Shen, R. Yu, Graphene-DNAzyme based biosensor for amplified fluorescence turn-on detection of Pb^{2+} with a high selectivity, Anal. Chem. 83 (2011) 5062–5066.
[11] S. Liu, W. Na, S. Pang, X. Su, Fluorescence detection of Pb^{2+} based on the DNA sequence functionalized CdS quantum dots, Biosens. Bioelectron. 58 (2014) 17–21.
[12] L. Wang, X.Y. Wang, G.S. Shi, C. Peng, Y.H. Ding, Thiacalixarene covalently functionalized multiwalled carbon nanotubes as chemically modified electrode material for detection of ultratrace Pb^{2+} ions, Anal. Chem. 84 (2012) 10560–10567.
[13] K.M. Zeinu, H.J. Hou, B.C. Liu, X.Q. Yuan, L. Huang, X.L. Zhu, J.P. Hu, J.K. Yang, S. Liang, X. Wu, A novel hollow sphere bismuth oxide doped mesoporous carbon nanocomposite material derived from sustainable biomass for picomolar electrochemical detection of lead and cadmium, J. Mater. Chem. A 4 (2016) 13967–13979.
[14] M.R. Awual, A novel facial composite adsorbent for enhanced copper(II) detection and removal from wastewater, Chem. Eng. J. 266 (2015) 368–375.
[15] M.R. Awual, New type mesoporous conjugate material for selective optical copper (II) ions monitoring & removal from polluted waters, Chem. Eng. J. 307 (2017) 85–94.
[16] M.R. Awual, Novel nanocomposite materials for efficient and selective mercury ions capturing from wastewater, Chem. Eng. J. 307 (2017) 456–465.
[17] M.R. Awual, Tsuyoshi Yaita, Shinichi Suzuki, Hideaki Shiwaku, Ultimate selenium (IV) monitoring and removal from water using a new class of organic ligand based composite adsorbent, J. Hazard. Mater. 291 (2015) 111–119.
[18] M.R. Awual, Solid phase sensitive palladium(II) ions detection and recovery using ligand based efficient conjugate nanomaterials, Chem. Eng. J. 300 (2016) 264–272.
[19] A. Shahat, M.R. Awual, M.A. Khaleque, M.Z. Alam, M. Naushad, A.M.S. Chowdhury, Large-pore diameter nano-adsorbent and its application for rapid lead(II) detection and removal from aqueous media, Chem. Eng. J. 273 (2015) 286–295.
[20] M.R. Awual, Assessing of lead(II) capturing from contaminated wastewater using ligand doped conjugate adsorbent, Chem. Eng. J. 289 (2016) 65–73.
[21] A. Shahat, H.M.A. Hassan, H.M.E. Azzazy, E.A. El-Sharkawy, H.M. Abdou, M.R. Awual, Novel hierarchical composite adsorbent for selective lead(II) ions capturing from wastewater samples, Chem. Eng. J. 332 (2018) 377–386.
[22] M.R. Awual, M.M. Hasan, Novel conjugate adsorbent for visual detection and removal of toxic lead(II) ions from water, Microporous Mesoporous Mater. 196 (2014) 261–269.
[23] Z. Lin, Y. Chen, X. Li, W. Fang, Pb^{2+} induced DNA conformational switch from hairpin to G-quadruplex: electrochemical detection of Pb^{2+}, Analyst 136 (2011) 2367–2372.
[24] S. Balasubramanian, L.H. Hurley, S. Neidle, Targeting G-quadruplexes in gene promoters: a novel anticancer strategy? Nat. Rev. Drug. Discov. 10 (2011) 261–275.
[25] F. Long, A. Zhu, H. Wang, Optofluidics-based DNA structure-competitive aptasensor for rapid on-site detection of lead(II) in an aquatic environment, Anal. Chim. Acta 849 (2014) 43–49.
[26] S. Pang, S. Liu, X. Su, An ultrasensitive sensing strategy for the detection of lead(II) ions based on the intermolecular G-quadruplex and graphene oxide, Sens. Actuators B: Chem. 208 (2015) 415–420.
[27] S. Dolati, M. Ramezani, K. Abnous, S.M. Taghdisi, Recent nucleic acid based biosensors for Pb^{2+} detection, Sens. Actuators B: Chem. 246 (2017) 864–878.
[28] C. Wang, H. Cheng, Y. Huang, Z. Xu, H. Lin, C. Zhang, Facile sonochemical synthesis of pH-responsive copper nanoclusters for selective and sensitive detection of Pb^{2+} in living cells, Analyst 140 (2015) 5634–5639.
[29] C. Wang, H. Cheng, Y. Sun, Z. Xu, H. Lin, Q. Lin, C. Zhang, Nanoclusters prepared from a silver/gold alloy as a fluorescent probe for selective and sensitive determination of lead(II), Microchim. Acta 182 (2015) 695–701.
[30] C. Wang, J. Wu, K. Jiang, M.G. Humphrey, C. Zhang, Stable Ag nanoclusters-based nano-sensors: rapid sonochemical synthesis and detecting Pb^{2+} in living cells, Sens. Actuators B: Chem. 238 (2017) 1136–1143.
[31] Y. Attia, M. Samer, Metal clusters: new era of hydrogen production, Renew. Sust. Energy Rev. 79 (2017) 878–892.
[32] I. Díez, R.H.A. Ras, Fluorescent silver nanoclusters, Nanoscale 3 (2011) 1963–1970.
[33] X. Xia, Y. Hao, S. Hu, J. Wang, Hairpin DNA probe with 5′-TCC/CCC-3′ overhangs for the creation of silver nanoclusters and miRNA assay, Biosens. Bioelectron. 51 (2014) 36–39.
[34] J.M. Obliosca, C. Liu, H.-C. Yeh, Fluorescent silver nanoclusters as DNA probes, Nanoscale 5 (2013) 8443–8461.
[35] L. Shang, S. Dong, G.U. Nienhaus, Ultra-small fluorescent metal nanoclusters: synthesis and biological applications, Nano Today 6 (2011) 401–418.
[36] G. Liu, D.-Q. Feng, X. Mu, W. Zheng, T. Chen, L. Qi, D. Li, DNA-functionalized silver nanoclusters as a chemopalette: tunable fluorescence for turn-on detection of cysteine, J. Mater. Chem. B 1 (2013) 2128–2131.
[37] Z. Huang, F. Pu, Y. Lin, J. Ren, X. Qu, Modulating DNA-templated silver nanoclusters for fluorescence turn-on detection of thiol compounds, Chem. Commun. 47 (2011) 3487–3489.
[38] J. Xu, C. Wei, The aptamer DNA-templated fluorescence silver nanoclusters: ATP detection and preliminary mechanism investigation, Biosens. Bioelectron. 87 (2017) 422–427.
[39] X. Liu, F. Wang, R. Aizen, O. Yehezkeli, I. Willner, Graphene oxide/nucleic-acid-stabilized silver nanoclusters: functional hybrid materials for optical aptamer sensing and multiplexed analysis of pathogenic DNAs, J. Am. Chem. Soc. 135 (2013) 11832–11839.
[40] L. Zhang, J. Zhu, S. Guo, T. Li, J. Li, E. Wang, Photoinduced electron transfer of DNA/Ag nanoclusters modulated by G-quadruplex/Hemin complex for the construction of versatile biosensors, J. Am. Chem. Soc. 135 (2013) 2403–2406.
[41] J. Yin, X. He, K. Wang, Z. Qing, X. Wu, H. Shi, X. Yang, One-step engineering of silver nanoclusters–aptamer assemblies as luminescent labels to target tumor cells, Nanoscale 4 (2012) 110–112.
[42] J. Yin, X. He, K. Wang, F. Xu, J. Shangguan, D. He, H. Shi, Label-free and turn-on aptamer strategy for cancer cells detection based on a DNA–silver nanocluster fluorescence upon recognition-induced hybridization, Anal. Chem. 85 (2013) 12011–12019.
[43] B. Yin, J. Ma, H.-N. Le, S. Wang, Z. Xu, B. Ye, A new mode to light up an adjacent DNA-scaffolded silver probe pair and its application for specific DNA detection, Chem. Commun. 50 (2014) 15991–15994.
[44] Y. Liu, X. Chang, Y. Guo, S. Meng, Biosorption and preconcentration of lead and cadmium on waste Chinese herb Pang Da Hai, J. Hazard. Mater. B 135 (2006) 389–394.
[45] B. Han, E. Wang, Oligonucleotide-stabilized fluorescent silver nanoclusters for sensitive detection of biothiols in biological fluids, Biosens. Bioelectron. 26 (2011) 2585–2589.
[46] W. Zhou, R. Saran, J. Liu, Metal sensing by DNA, Chem. Rev. 117 (2017) 8272–8325.
[47] T. Li, E. Wang, S. Dong, Potassium–lead-switched G-quadruplexes: a new class of DNA logic gates, J. Am. Chem. Soc. 131 (2009) 15082–15083.
[48] S. Liu, W. Na, S. Pang, X. Su, Fluorescence detection of Pb^{2+} based on the DNA sequence functionalized CdS quantum dots, Biosens. Bioelectron. 58 (2014) 17–21.
[49] P.R. Majhi, R.H. Shafer, Characterization of an unusual folding pattern in a catalytically active guanine quadruplex structure, Biopolymers 82 (2006) 558–569.
[50] C.-L. Li, K.-T. Liu, Y.-W. Lin, H.-T. Chang, Fluorescence detection of lead(II) ions through their induced catalytic activity of DNAzymes, Anal. Chem. 83 (2011) 225–230.
[51] W. Wang, Y. Jin, Y. Zhao, X. Yue, C. Zhang, Single-labeled hairpin probe for highly specific and sensitive detection of lead(II) based on the fluorescence quenching of deoxyguanosine and G-quartet, Biosens. Bioelectron. 41 (2013) 137–142.
[52] X. Liu, R. Hu, Z. Gao, N. Shao, Photoluminescence mechanism of DNA-templated silver nanoclusters: coupling between surface plasmon and emitter and sensing of lysozyme, Langmuir 31 (2015) 5859–5867.
[53] E. Shaviv, O. Schubert, M. Alves-Santos, G. Goldoni, R.D. Felice, F. Vallée, N. Fatti, U. Banin, C. Sönnichsen, Absorption properties of metal-semiconductor hybrid nanoparticles, ACS Nano 5 (2011) 4712–4719.
[54] Y. Guo, J. Li, X. Zhang, Y. Tang, A sensitive biosensor with a DNAzyme for lead(II) detection based on fluorescence turn-on, Analyst 140 (2015) 4642–4647.
[55] Z. Wang, B. Chen, J. Duan, T. Hao, X. Jiang, Z. Guo, S. Wang, A test strip for lead(II) based on gold nanoparticles multi-functionalized by DNAzyme and barcode DNA, J. Anal. Chem. 70 (2015) 339–345.
[56] T. Li, S. Dong, E. Wang, A lead(II)-driven DNA molecular device for turn-on fluorescence detection of lead(II) ion with high selectivity and sensitivity, J. Am. Chem. Soc. 132 (2010) 13156–13157.
[57] S. DasGupta, S.A. Shelke, N.-S. Li, J.A. Piccirilli, Spinach RNA aptamer detects lead (II) with high selectivity, Chem. Commun. 51 (2015) 9034–9037.
[58] L. Chun, C.-Z. Huang, Detection of lead ions in water based on the surface energy transfer between gold nanoparticles and fluorescent dyes, Chin. J. Anal. Chem. 42 (2014) 1195–1198.
[59] S. Zhan, Y. Wu, Y. Luo, L. Liu, L. He, H. Xing, P. Zhou, Label-free fluorescent sensor for lead ion detection based on lead(II)-stabilized G-quadruplex formation, Anal. Biochem. 462 (2014) 19–25.
[60] X.-R. Song, N. Goswami, H.-H. Yang, Jianping Xie, Functionalization of metal nanoclusters for biomedical applications, Analyst 141 (2016) 3126–3140.
[61] J.T. Petty, S.P. Story, J.-C. Hsiang, R.M. Dickson, DNA-templated molecular silver fluorophores, J. Phys. Chem. Lett. 4 (2013) 1148–1155.
[62] C. Li, C. Wei, DNA-templated silver nanocluster as a label-free fluorescent probe for the highly sensitive and selective detection of mercury ions, Sens. Actuators B: Chem. 242 (2017) 563–568.
[63] C. Wang, J. Wu, K. Jiang, M.G. Humphrey, C. Zhang, Stable Ag nanoclusters-based nano-sensors: rapid sonochemical synthesis and detecting Pb^{2+} in living cells, Sens. Actuators B: Chem. 238 (2017) 1136–1143.
[64] B. Adhikari, A. Banerjee, Facile synthesis of water-soluble fluorescent silver nanoclusters and Hg^{II} sensing, Chem. Mater. 22 (2010) 4364–4371.